Volume:37 No:2 2024

e-ISSN-2791-7185

TURKISH JOURNAL OF NUCLEAR SCIENCES

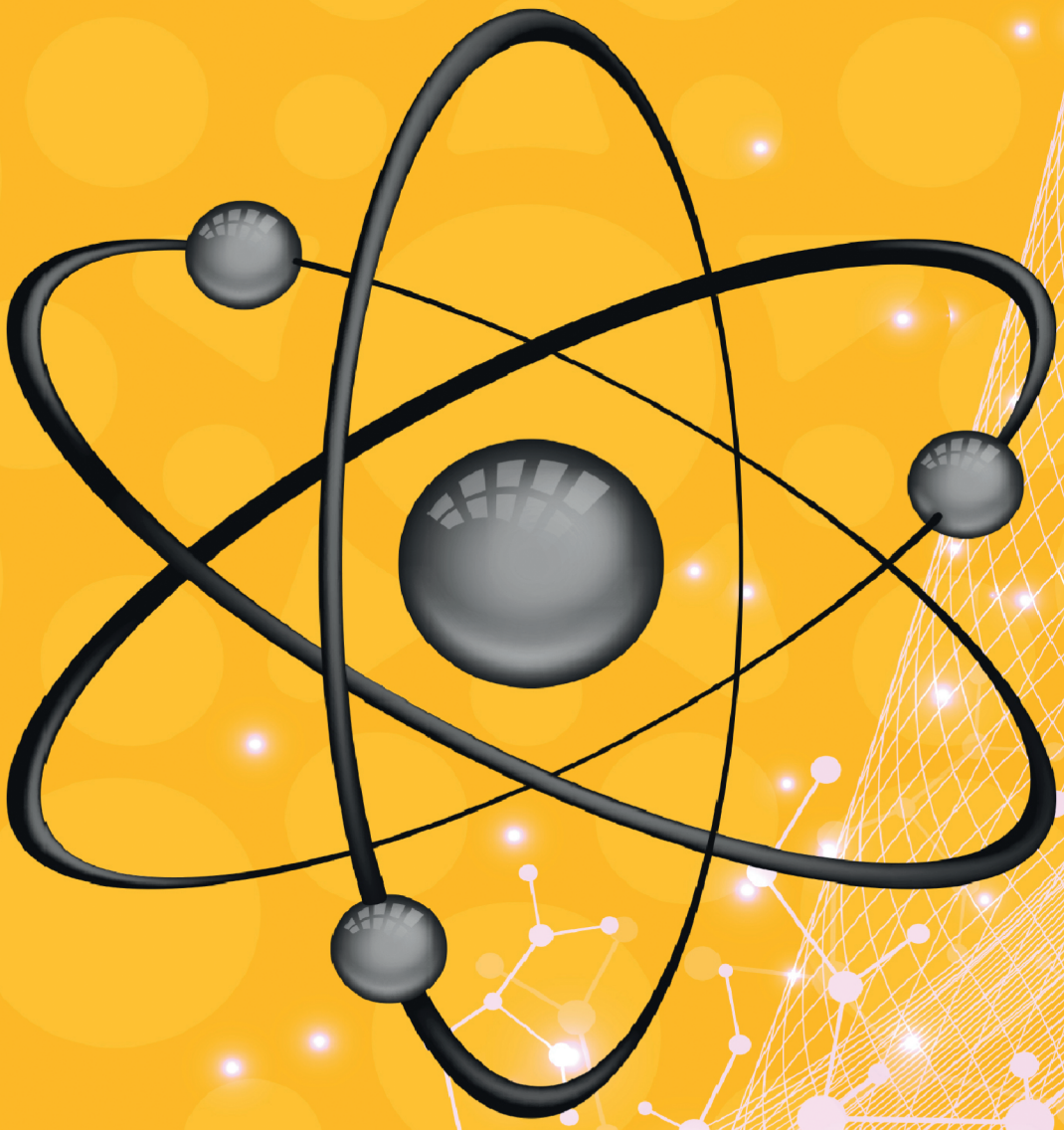

e-ISSN: 2791-7185

TURKISH JOURNAL OF NUCLEAR SCIENCES

CİLT VOL **37** **SAYI** ISSUE **02** **YIL** YEAR **2024**

Yayıncı/Publisher
TENMAK Akademi ve Yayınlar Koordinatörlüğü

Yayın İdare Adresi/Adress of Publication Manager
Ankara Üniversitesi Beşevler Kampüsü Emniyet Mahallesi
Yenimahalle, 06560, Ankara, Türkiye
Tel: (0312) 212 62 30
Fax: (0312) 295 87 61
E-posta: journal@tenmak.gov.tr
Web: https://dergipark.org.tr/tr/pub/tjns

Yayın Türü/Type of Publication: Yaygın süreli yayın
Yayın Aralığı/Range of Publication: 6 Aylık
Yayın Tarihi/Publication Date: 31/12/2024

Turkish Journal of Nuclear Sciences ulusal ve uluslararası hakemli bir dergidir. Dergi elektronik ortamda Haziran ve Aralık aylarında olmak üzere yılda iki kez yayımlanmaktadır. Derginin yazım kılavuzuna, telif hakkı devir formuna ve yayınlanan makalelere https:// https://dergipark.org.tr/tjns adresinden ulaşılabilir./ Turkish Journal of Nuclear Sciences is National and International refereed journal. Journal has been published twice a year, in June and December, only electronically .Please visit the Journal website https:// https://dergipark.org.tr/tjns for writing rules, copyright form and published articles.

ANKARA
ARALIK 2024 / DECEMBER 2024

TENMAK

TURKISH ENERGY, NUCLEAR AND MINERAL RESEARCH AGENCY

TURKISH JOURNAL OF NUCLEAR SCIENCES

E-ISSN: 2791-7185

https://dergipark.org.tr/tr/pub/tjns

İÇİNDEKİLER/CONTENTS

TENMAK

TURKISH ENERGY, NUCLEAR AND MINERAL RESEARCH AGENCY
TURKISH JOURNAL OF NUCLEAR SCIENCES
E-ISSN: 2791-7185
https://dergipark.org.tr/tr/pub/tjns

Antimicrobial Photodynamic Therapy Using Indocyanine Green Loaded FDG Conjugated Cubic Iron Oxide (C-Fe_3O_4) Nanoparticles

Önder Bakır [1,*], Kadriye Büşra Karatay [1], Elif Tutun [1], Volkan Yasakçı [1], Gillian Pearce [2], Perihan Unak [1]

[1] Ege University, Institute of Nuclear Sciences, Department of Nuclear Applications, 35100 Bornova, Izmir, Türkiye
[1] Aston University, School of Engineering and Applied Sciences, Birmingham, B1 1DD, West Midlands, UK

ARTICLE INFO

Article History:
Received October 1, 2024
Available online December 31, 2024

Research Article

Keywords:
- *Escherichia coli* (*E. coli*)
- Green Fluorescence Protein (GFP)
- Near-infrared (NIR)
- Photodynamic therapy
- Superparamagnetic iron oxide nanoparticles (SPIONs)

ABSTRACT

Our aim is to provide nanostructures combining photodynamic therapy (PDT) and low-dose radiation therapy (RT) to target Escherichia coli (*E. coli*) and Green Fluorescence Protein-E coli bacteria (GFP-*E. coli*). To accomplish this, we synthesized cubic iron oxide nanoparticles conjugated with 2-deoxy-2-[fluorine-19] fluoro-D-glucose (FDG) and loaded them with indocyanine green (ICG) (referred to as ICG@FDG-MNPs). ICG, which has the potential for PDT, was incorporated into ICG@FDG-MNPs to enable effective combined therapy approach targeting *E. coli* bacteria using an LED beam and LINAC-X-ray source treatment. PDT/RT studies demonstrated that when the nanoconjugate was initially stimulated with the LED beam on *E. coli* and Green Fluorescence Protein-*E. coli* bacteria, radiation damage increased, ultimately leading to bacterial death.

1. Introduction

Bacterial infections caused by pathogens are deadly diseases that have a significant impact on human health and mortality. Significant advances have been made in the treatment of bacterial infections over the last few decades. However, the effectiveness of these antimicrobial agents diminishes over time due to the development of resistant bacteria [1]. Antibiotic-resistant pathogens, including Escherichia coli, caused more than 250,000 deaths due to bacterial infection syndrome worldwide in 2019 [2]. Recent estimates suggest that deaths from drug-resistant bacterial infections will continue to increase in the next few decades [2]. The cocktail of magnetic nanoparticles (MNPs) induces robust immune responses against its components [3]. MNPs are utilized in various therapeutic and diagnostic methods. One of these methods is PDT, which gained importance in recent years, particularly in non-oncological antitumor treatment, as it offers a potential alternative with fewer side effects than existing treatments [4]. The basis of this therapy method is to deliver LED light with wavelengths between 400-700 nm to target cells using a photosensitizing (PS) molecule. This approach aims to enhance the drug's efficacy by inducing apoptosis in the target cell through light stimulation [5]. The fact that PDT induces apoptosis of target cells solely with the assistance of free oxygen has allowed this therapy method to be utilized in treatment of both bacterial infections and cancer [6]. Particularly, current applications in the treatment of multidrug-resistant bacterial infections demonstrate the effectiveness of PDT [7, 8].

There are two different reaction pathways involved in the activity of PDT. The first pathway is photosensitizer that reacts with its oxidizing substrate and second pathway is photosensitizer reacts with ground-state triplet oxygen. These pathways cause formation of reactive oxygen radicals [7]. Current studies suggest the use of nanoparticles to enhance the efficiency of photosensitizers, which is the main component of these reactions [9, 10]. This is because photosensitizers are often hydrophobic and require a carrier system for more effective biodistribution [11]. Nanoparticles conjugated with various photosensitizers have shown significant potential in antimicrobial photodynamic therapy [6, 12].

MNPs promise in the diagnosis and treatment of not only cancer but also bacterial infections [13]. They have gained significant attention in the field of antimicrobial therapy due to their unique properties, which distinguish them from conventional nanoparticles. Their ability to be guided by external magnetic fields and their high surface area make them promising candidates for targeted bacterial delivery and enhanced antimicrobial effects. One of the primary advantages of MNPs is their ability to be directed to specific sites using external magnetic fields. This feature allows for precise localization of nanoparticles

*Corresponding author: bakironder@gmail.com

at infection sites, which improves the efficiency of treatment by ensuring that therapeutic agents are concentrated where they are most needed. The use of magnetic fields enables MNPs to accumulate in targeted tissues, reducing off-target effects in healthy areas [14]. Studies have demonstrated that this magnetic targeting can significantly increase the therapeutic potential of nanoparticles by increasing their local concentration in infected areas, thereby improving antimicrobial efficacy [15]. Additionally, the prolonged retention of MNPs at the site of infection increases their interaction time with bacterial cells, potentially enhancing the treatment outcome. Magnetic nanoparticles can exert antimicrobial effects through several mechanisms. Their ability to disrupt bacterial cell membranes and interfere with cellular processes is a key factor in their antimicrobial activity. Furthermore, MNPs can be functionalized with antimicrobial agents, such as antibiotics or peptides, which can be specifically delivered to the infection site under the influence of a magnetic field. This ensures that antimicrobial agents are concentrated in infection, reducing systemic exposure and minimizing side effects [16]. The localized application of these agents also improves their efficiency in combating resistant bacterial strains [17]. Moreover, MNPs can generate reactive oxygen species (ROS) or induce mechanical damage to bacterial cells, which contributes to their bactericidal effect [15, 18]. This multifaceted approach makes MNPs highly effective in combating bacterial infections, particularly those caused by antibiotic-resistant strains. This functionalization capability enhances the specificity of MNPs in targeting bacterial pathogens and enables the development of customized treatments tailored to specific types of infections or antibiotic-resistant bacteria [16, 19]

MNPs exhibit excellent magnetic saturation due to their strong ferromagnetic properties. They are chemically stable and biocompatible. However, magnetic nanoparticles without surface coating tend to aggregate due to their high surface energies [20]. Polymeric materials, such as polyethylene glycol (PEG), have been widely employed for coating superparamagnetic iron oxide nanoparticles (SPIONs). This is because PEG exhibits lower toxicity, high colloidal stability, biocompatibility, and reduced bacterial adhesion on surfaces. Additionally, the coating or modification of MNPs with PEG has improved morphology, properties, and targeting abilities [21]. Due to their low toxicity, magnetic nanoparticles have recently been actively studied for their antibacterial properties. SPIONs can be used as targeting to disease both porphyrin and non- photosensitizers (PSs) using external magnetic field. This approach helps limit the biodistribution of PSs in non-targeted tissue [11, 22]. However, the limited activity of PSs carried by nanoparticles may also be attributed to insufficient light wavelength for cell penetration and low affinity in bacterial cells, which could potentially pave the way for secondary infections [23]. Surface modifications are implemented on nanoparticles to prevent low selectivity, increase bioavailability and biodistribution, and enhance affinity for bacterial cells. Most photosensitizing substances, such as ICG and methylene blue, are produced with a cationic charge to enhance their affinity for bacteria [23].

Fluorodeoxyglucose (FDG), is a glucose analog commonly used in positron emission tomography (PET) imaging for monitoring metabolic activity. FDG is structurally similar to glucose and is taken up by cells through glucose transporters. Once inside the cell, FDG is phosphorylated, but unlike glucose, it is not further metabolized and thus accumulates within the cell. This characteristic allows FDG to accumulate in areas of high metabolic activity, such as cancer cells or infected tissues, making it useful for imaging these areas. The ability of FDG to accumulate in metabolically active cells is crucial for its role in diagnostic imaging and targeted therapies [24]. The mechanism of FDG-coated MNP uptake by bacteria relies on the ability of FDG to be transported into cells via glucose transporters, which are integral membrane proteins responsible for facilitating glucose entry into cells. Because FDG is structurally similar to glucose, it is recognized and transported by these glucose transporters. Once FDG-coated MNPs enter bacterial cells, the magnetic properties of the nanoparticles allow them to be guided to specific areas using an external magnetic field. This external guidance can help increase the accumulation of the nanoparticles at infection sites, potentially enhancing therapeutic efficacy. The accumulation of FDG within bacterial cells occurs because bacteria, particularly in infected or active metabolic states, have an increased demand for glucose, leading to greater FDG uptake.

The uptake of FDG by bacteria is generally specific to metabolically active cells and depends on the presence of glucose transporters. Bacteria with high metabolic activity, such as those found in infected tissues, tend to take up glucose and its analogs like FDG more efficiently. However, this uptake is not entirely specific to one bacterial species; it depends on the presence of functional glucose transporters on the bacterial surface and the metabolic activity of the bacteria.

While FDG is preferentially taken up by bacteria that are metabolically active and have glucose transporters, not all bacterial species exhibit the same level of uptake. Some bacteria may have fewer glucose transporters, or their metabolic activity may not be sufficient to drive significant FDG uptake. Therefore, while FDG-coated MNPs are more efficiently taken up by certain bacterial species, the process is not entirely specific to a single bacterial type. The efficiency of uptake can vary based on the bacteria's metabolic characteristics and their expression of glucose transporters [25, 26]. Recent studies demonstrate that FDG is a powerful agent for monitoring biochemical and physiological processes in *E. coli*. Matsumoto and co-workers investigated FDG's

conversion to fluorescein by the β-galactosidase enzyme in *E. coli*. A novel microfluidic device was used to analyze efflux pump interactions, aiding in the understanding of bacterial resistance mechanisms [27]. In another study, Landon and co-workers investigates the effects of β-defensins on *E. coli*, using fluorescence microscopy to track FDG-related processes like membrane permeability and bacterial growth dynamics under physiological conditions [28]. These studies highlight FDG's role in visualizing and understanding bacterial processes, particularly in *E. coli.*

Green fluorescent proteins (GFPs) have been extensively utilized as spectroscopic and microscopic probes in a wide range of physiological systems. In this study, E. coli bacteria containing GFP were used to investigate the efficacy of fluorescent photons emitted by GFP in photodynamic therapy [29]. The present report describes the investigation of the antimicrobial efficacy of ICG@FDG-MNPs, which have enhanced bioavailability due to various surface and structural modifications, in the combined treatment approach of PDT/RT.

2. Methods

2.1. Chemicals and Equipment

The chemicals used in cubic iron oxide nanoparticle synthesis and tetraethyl orthosilicate (TEOS) were supplied from Merck KGaA (Darmstadt, Germany).

NaF and 2-mercaptoethanol were obtained from Fluka (Germany). PEG, NHS, THF, NH_3 (25%), mannose triflate, kryptofix, K_2CO_3, $NaCNBH_3$, ethylenediamine, DMF, APTES, ICG, CDI, MES, NaCl and oleic acid were purchased from Sigma Aldrich (Germany). *Escherichia coli* (*E. coli*) and green fluorescent protein *Escherichia coli* (GFP-*E. coli*) bacteria were supplied from Ege University Department of Biochemistry in Izmir, Turkey, and LINAC (TrueBeam) irradiation was performed at Medicana Hospital in Izmir, Turkey.

Size and zeta potential measurements of nanoparticles and viability analyses of bacteria were carried out with the following devices located at the Ege University Institute of Nuclear Sciences: Zeta Sizer (Malvern Nano ZS DLS, Malvern, UK), A plate reader (Biotek, Elx800 Universal Absorbance Microplate Reader, USA), a microscope (Leica Microsystems, Germany), a hemocytometer (Carl Zeiss, Jena Germany), an EVOS XL imaging system (Thermofisher, UK).

2.2. Chemicals and Equipment

Synthesis of iron oxide nanoparticles was prepared according to Martinez-Bobueta *et al*. [12]. For the synthesis, 0.353 g (1 mmol) Fe(acac)3 was mixed with 0.688 g (4 mmol) decanoic acid in 25 mL dibenzyl ether. After heating at 60°C (30 min), the solution temperature was increased to 200°C and stirred with a magnetic stirrer under argon flow at 800 rpm for 2h. At the end of 2 hours, the solution temperature was increased to reflux temperature (300oC) and stirred at 800 rpm for 1h. The solution was cooled for 1 h and the nanoparticles were washed 3 times with ethanol using magnets and redispersed in ethanol.

Surface modifications with silica and silane were synthesized by modifying our previous method [30]. C-Fe_3O_4 nanoparticles (100 mg) were dispersed using ultrasonication in a mixture of ethanol and distilled water with a total volume of 10 mL. pH was adjusted to 9 with ammonia (NH_3) solution. 2.5 mL TEOS was added dropwise, and the mixture was heated to 40°C under reflux. The solution was stirred at this temperature at 600 rpm for 12 hours. In the second step, a similar process was used for the synthesis of C-Fe_3O_4@SiO_2-NH_2 nanoparticles. For this, 3 mL of APTES was added to the C-Fe_3O_4@SiO_2 nanoparticles (100 mg) dropwise, and the mixture was stirred under reflux at 600 rpm at 60°C for 14 h. In both steps, the precipitate was separated by magnetization and washed several times with ethanol. Nanoparticles were stored in ethanol at 4°C.

PEGylation was performed following the method described by Zhang's report [31]. Prior to surface modification, the C-Fe_3O_4@SiO_2-NH_2 nanoparticles were dried to remove any adsorbed water. 12 mg of PEG (Poly (ethylene glycol) 2-aminoethyl ether acetic acid) was dissolved in 3 mL of THF. The C-Fe_3O_4@SiO_2-NH_2 nanoparticles, dispersed in THF, were mixed with a 1:1 weight ratio of PEG overnight at 60°C. Then, distilled water was added to the mixture with ultrasonic agitation, and THF was allowed to evaporate overnight.

Synthesis of FDG and conjugation with MNPs were carried out similarly to our previous method [24, 32]. ICG-bound FDG-MNP was synthesized using previously reported methods [24, 33]. FDG-MNP was activated by CDI and then bound to the sulfo groups of ICG through the OH groups on the nanoparticle surface.

2.3. Characterization of Synthesized Nanoparticles

The hydrodynamic diameters were analyzed using Malvern Nano-ZS DLS. The nanoparticles were kept in an ultrasonic bath for 30 minutes and then passed through 0.45 μm filters. Results are expressed as mean ± standard deviation.

SEM and TEM images were taken at Ege University Central Research Laboratory (MATAL) and Eskişehir Osmangazi University Central Research Laboratory Application and Research Center (ARUM). For SEM imaging, FDG-MNP was dried and dissolved in ethanol and coated with 80% Au and 20% Pd. The sample was prepared by drying a carbon-coated copper grid in a dilute ethanol suspension at room temperature. High-resolution TEM images were obtained by dispersing the powder in methanol, stirring with ultrasound for

a few minutes, followed by pipetting one drop onto a carbon support film on a 3 mm copper grid.

2.4. Photodynamic Therapy/Radiotherapy

Four different working groups were formed for PDT and RT experiments of ICG@FDG-MNPs. 1-2 ml of each bacterial sample (sterile saline, PBS, dH_2O) was taken and read at 620 nm to determine the Mc Farland value. An absorbance value of 0.1 corresponds to a Mc Farland turbidity value of 0.5 Mc Farland pattern. *E. coli* (*Escherichia coli*) and GFP-*E. coli* (Green Fluorescent Protein *Escherichia coli*) bacteria were inoculated in Nutrient Broth medium with 0.5 Mc Farland pattern turbidity on 96 well plates, respectively, concentrations of FDG-MNP (1, 2, 10, 20, 100 µg/ µL) (Fig 2) was added in duplicate, and absorbance values were read at 620 nm. After the 24-hour incubation period, the absorbance values at 620 nm in each well were measured again to determine the bacterial proliferation. A graph was then plotted using the differences in absorbance. Photodynamic LED light irradiation with a wavelength of 400-700 nm for 5 minutes at 30 cm. This was followed by the administration of a 1 Gy X-ray dose 30 minutes later for 2 minutes. This was conducted with four different sets of samples, each undergoing various combinations of the two treatment methods [34]. The first group was initially exposed to light, followed by radiation after 24 hours. In the second group, the order of exposure was reversed, with radiation administered first, followed by LED light. The LED beam source used had wavelengths of 400-700 nm and a power of 5.1 Jcm^{-2}. The third group was only exposed to an LED beam, while the fourth group was exposed only to radiation. Bacteria-free medium was used as a negative control and only bacteria in the medium without any other substances (like antibiotics,nanoparticles etc.) were used as positive control and exposed to all photodynamic therapy and radiotherapy conditions in the same manner. Viabilities (%) were calculated by dividing the measured absorbance value by the control value as the percentage value. The absorbance of the negative control was considered zero [35, 36].

2.5. Statistical Analysis

The statistical significance was assessed using the Graph Pad Prism version 5.0 for Windows program via one-way ANOVA and linear regression [37]. A one-way analysis of variance was used to compare differences between the *E. Coli* and GFP-*E. Coli* treated groups. Data was expressed as the mean ± standard deviation and $P < 0.05$ was considered to indicate a statistically significant difference.

3. Results and Discussion

3.1. Characterizations

Fig. 1a and Fig. 1b show SEM and TEM images of FDG-MNPs, respectively. The average hydrodynamic diameters for C-Fe3O4 and C-Fe_3O_4@SiO_2 were measured as 159.0±12.0 nm and 162.6±4.0 nm, respectively (Fig. 1c). The hydrodynamic sizes of C-Fe_3O_4@SiO_2-NH_2-PEG nanoparticles and FDG-MNPs were found to be 256.1±9.0 nm and 314.0±4.0 nm, respectively. The decrease in zeta potential from C-Fe_3O_4 to C-Fe_3O_4@SiO_2 is likely due to the surface charge of the silica molecules present on the surface of the Fe_3O_4 nanoparticles. This surface charge reduces the agglomeration of nanoparticles in aqueous media, enabling the magnetic nanoparticles to retain their colloidal structure. SEM and TEM images revealed that the particle size and shape exhibited a smooth, homogeneous spherical morphology, consistent with the literature [38]. Based on the images, the nanoconjugate exhibited a smooth and round surface (Fig. 1a), and the surface coating did not interfere with the structure of the cubic-shaped iron core (Fig. 1b). The surface coating resulted in an increase in the nanoparticle size which was an expected outcome. These results are consistent with our previous studies [24, 32].

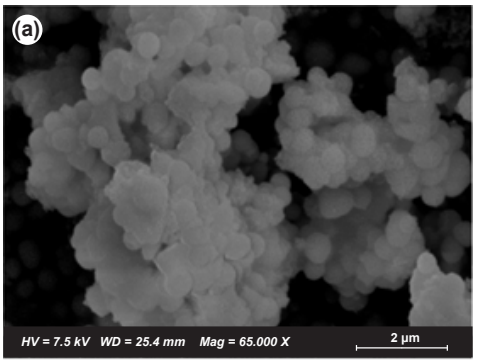

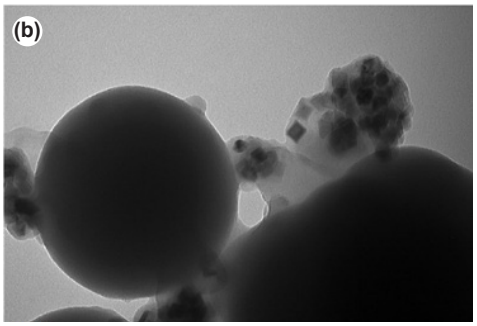

(c)

Nanoconjugates	Hydrodinamic Diameter (d.nm)	Agv. Zeta Potantial (mV)
C-Fe_3O_4	159.0 ± 12.0	+2.51 ± 1.0
C-Fe_3O_4-SiO_2	162.6 ± 4.0	-19.1± 0.6
C-Fe_3O_4-SiO_2-NH_2	163.2 ± 5.0	-36.0± 0.7
C-Fe_3O_4-SiO_2-NH_2PEG	256.1 ± 9.0	-20.4± 1.2
C-Fe_3O_4-SiO_2-NH_2PEG-FDG	314.0 ± 4.0	-24.0± 0.3
C-Fe_3O_4-SiO_2-NH_2PEG-FDG@ICG	120.5 ± 4.5	-16.4± 1.55

Figure 1. (a) SEM image of FDG-MNPs, (b) TEM image of FDG-MNPs and (c) the average hydrodynamic diameters and zeta potential values of nanoparticles.

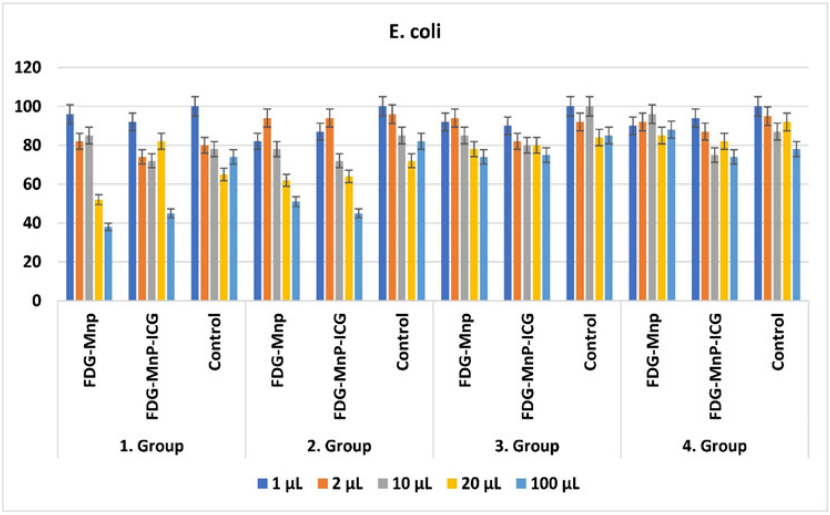

Figure 2. Antimicrobial efficacies of E. Coli in different rates FDG-MNP and ICG@ FDG-MNP concentrations (The 1st group: light first and then radiation, The 2nd group: first radiation and then LED light, The 3rd group: only exposed to an LED beam and 4th group: only exposed to radiation.)

3.2. Photodynamic Therapy/Radiotherapy

Photodynamic therapy has been proven to be effective against biofilm-forming strains and to treat bacteria without resistance to antibiotics [34]. However, its application in deep infections is limited due to the restricted penetration of light [39]. To overcome this limitation, combined treatment methods including photodynamic therapy, are recommended, as current studies have demonstrated their stronger bactericidal effect [40, 41]. In our current study, we observed that the vitality rate for the 1st and 2nd groups, in which light and radiation were applied simultaneously, was lower than the 3rd and 4th groups, where only light or only radiation was applied. Kunz *et al*. demonstrated the effects of PDT on Gram-negative bacteria using LED light at a wavelength of 460 nm using 0.1% riboflavin photosensitizer [42]. Although the vitality rate of *E. coli* bacteria exposed to photodynamic therapy alone (3*rd* group) was higher than that of the groups exposed to combined therapy, the significant decrease in this rate compared to the control group supports the potential use of photodynamic therapy in Gram-negative bacterial biofilms.

In recent years, the use of nanoparticles has become widespread in antibacterial photodynamic therapy and combined therapy methods. Various methods involving nanoparticles have been employed, such as utilizing modified nanoparticles as photosensitizers or as transport systems to enhance the efficient delivery of photosensitizers to bacterial cells [6, 43]. Mohanta *et al*. demonstrated the antibacterial and antibiofilm effect of silver nanoparticles on Gram-negative and multi-drug resistant *E. coli* bacteria microbiota [44].

Aras *et al*. reported that conjugation of ICG with FDG-MNPs provides more accurate and positive results in tumor monitoring [45]. In our study, when evaluating the results, the bactericidal effect of FDG-MNPs and ICG@FDG-MNPs was found to be higher than that of the control groups (see Fig 2 and Fig 3).

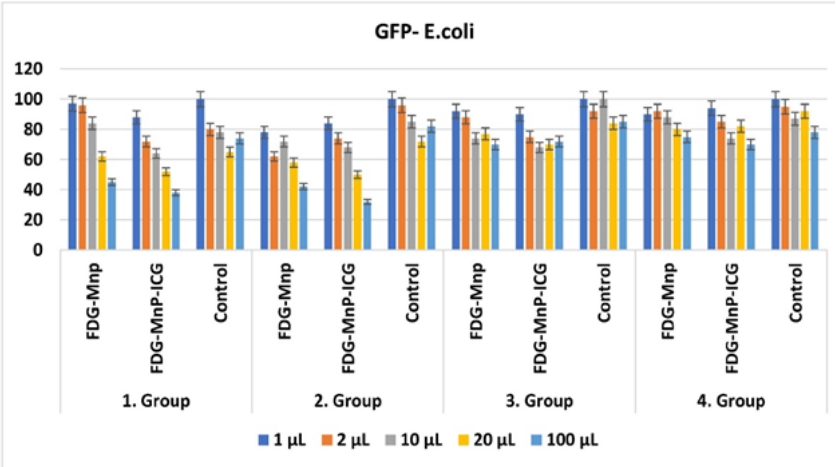

Figure 3. Antimicrobial efficacies of GFP-E.Coli in different rates FDG-MNP and ICG@ FDG-MNP concentrations (The 1st group: light first and then radiation, The 2nd group: first radiation and then LED light, The 3rd group: only exposed to an LED beam and 4th group: only exposed to radiation.)

Combined photodynamic and low-dose radiation therapy for cancer cell damage has been previously reported [34, 35, 46]. Tekin *et al*. reported that PC3 and LNCaP cell viability was significantly reduced when light and radiation were applied using SPHINX-conjugated Pt@TiO nanoparticles. Our study also demonstrated the antibacterial efficacy of the combined treatment method developed and tested for cancer. Radiation creates reactive oxygen species in the living media and causes excitation and ionization. ICG as a light-sensitive dye activates reactive oxygen species (ROS) with radiation in the living media. The effect of light synergistically enhances the radiation damage of ROS [35].

Bacteria-free medium was used as a negative control, and only bacteria in the medium without any antibiotics or nanoparticles etc. were used as a positive control group. In the control group, bacterial damage decreases with increasing concentration. Bilici *et al*. reported that ICG-conjugated SPIONs in photodynamic therapy methods, incorporating PDT and photothermal therapy (PTT), provide an effective and alternative antibacterial therapy even in the absence of antibiotics [47]. Magesan *et al*. reported that the Fe_2O_3-TiO_2 nanocomposites on bacteria have remarkably antibacterial activity against *E. coli* [48]. Photodynamic therapy using nanoparticular systems may be a new solution for the treatment of drug-resistant bacterial infections [48, 49].

The increase in antibiotic resistance in recent years has sparked increased interest in non-antibiotic treatment methods for bacterial infections. Photodynamic therapy (PDI) has received attention in recent years due to its high effectiveness. Furthermore, low-dose X-irradiation shows potential as a more effective treatment when combined with photodynamic therapy. Radiation therapy is commonly used for cancer treatment, but its application in the treatment of bacterial infections, such as caused by *E. coli*, is a developing area of research. The concept of using radiation to kill bacteria or prevent their growth isn't new, and in some cases, ultraviolet (UV) or X-rays have been tested as potential antibacterial agents [50-52]. The use of radiation as a clinical tool for treating infections is still an experimental area and studies are limited in the literature concerning the bacteria and clinical radiotherapy applications. Typically, radiation therapy is generally combined with other agents (such as antibiotics) to increase effectiveness, and its safety and efficacy depend heavily on the dose and type of radiation used, as well as the duration of exposure [53-55]. However, ionizing radiation, such as X-rays and gamma rays, is widely used in clinical settings for local treatment. For instance, in 1982, Luckey proposed that low dose ionizing radiation (LDI) could be beneficial to animal health and survival. This hypothesis has since been supported by several studies, reinforcing the potential positive impacts of LDI on health [56-58] (In our previous studies, we reported that the combined use of different nanoparticles, low-dose X-ray therapy, and photodynamic therapy yields effective results in various cancers [35, 36, 59]. Antibacterial resistance poses a serious threat to human health [38]. The rapid proliferation and mutation of bacteria, along with the overuse of antibiotics and their inappropriate release into the environment, have significantly contributed to the emergence and spread of antibiotic-resistant bacteria. It is crucial to explore innovative therapeutic approaches to overcome antibiotic resistance [5]. Among these approaches, photodynamic therapy (PDT), which is a clinically proven antibacterial therapy, stands out as one of the innovative methods [6]. This approach relies on the interaction of a non-toxic photosensitizer (PS), oxygen, and light of the appropriate wavelength to generate highly reactive oxygen species (ROS). These ROS instantly react with surrounding biomolecules and damage their bioactive components, such as cytoplasmic membranes. In this way, it leads to irreversible cell inactivation, affecting intracellular proteins and DNA [7]. Various compounds such as TiO_2 [8], fullerenes, phenylenes [10], methylene blue [11, 12] and porphyrins [23, 24] have been used for this purpose. However, due to the differences in structure and physicochemical properties of PSs, as well as the variability in bacterial membrane structures, PSs demonstrate activity against specific bacterial species or strains. Therefore, the design and discovery of new PSs that can achieve higher efficiency against a broader range of bacteria remain a significant challenge.

The treatment of bacterial biofilms presents a significant challenge in wounds, primarily due to the limited penetration of antibiotics. Wounds containing biofilms of antibiotic-resistant bacteria have an even poorer prognosis. To enhance biocompatibility and reduce toxicity, we modified our nanoparticles with PEG in a simple one-step reaction. We propose a combined therapy approach that involves low-dose X-ray therapy in conjunction with photodynamic therapy, where the external application of our pegylated FDG-MNP nanoparticles deactivates biofilms and resistance mechanisms [59].

MNPs have other innovative potential applications in (*i*) therapy with hyperthermia [32] and (*ii*) in imaging as magnetic resonance imaging (MRI) probes [60]. Mahandran *et al*. demonstrated the utility of FDG MNPs in magnetic hyperthermia and cancer therapy. Magnetic hyperthermia is based on the local application of a magnetic field, causing damage to the tumor by increasing its temperature above body temperature [32]. Photodynamic therapy combined with low-dose radiotherapy that damages cancer or bacterial cells via reactive oxygen species (ROS) may be more effective in common bacterial infections resistant to antibiotics.

The nanoparticles exhibit lower oxidation and relatively low toxicity in comparison to many other materials, such as iron, nickel, and cobalt. Moreover, new bioconjugates can be developed to enhance their bioavailability, such as the use of FDG labeled with

nonradioactive ^{19}F, as a conjugate to increase their affinity for both cancer cells [61, 62] and infections [63]. This research can establish the safety of its *in vivo* applications and explore its potential in cancer treatment, while also unlocking possibilities for other medical applications. The obtained results would offer valuable guidance for the future development of multifunctional agents and the further optimization of their diagnostic performance in clinical settings.

4. Conclusions

In conclusion, we have observed that the ICG@FDG-MNP exhibits greater efficacy, particularly against GFP-*E. coli* bacterial strains. Furthermore, the combined therapy approach proves to be more effective in terms of its antibacterial effects compared to radiotherapy or photodynamic therapy alone. In future studies, we recommend conducting more comprehensive investigations into the antibacterial effects of photosensitizers and further defining the effectiveness of combined treatment methods for infectious diseases.

5. Acknowledgements

Authors thank Prof Dr Serap Evran from Ege University, Department of Biochemistry in Izmir-Turkey for the green fluorescent bacteria she gifted and Dr. Funda Manalp and Alpman Manalp for LINAC irradiation in Medicana Hospital, Izmir/Turkey. The work was partially presented at the International Nuclear Sciences and Technologies Conference (INSTEC-22).

6. Conflicts of Interest

The authors declare no conflict of interest.

Abbreviations	Descriptions
C-Fe_3O_4	Cubic iron oxide
C-Fe_3O_4-SiO_2	Cubic iron oxide coated with TEOS
C-Fe_3O_4-SiO_2-NH_2	Cubic iron oxide coated with TEOS and APTES
C-Fe_3O_4-SiO_2-NH_2-PEG	Cubic iron oxide coated with TEOS, APTES and PEG
FDG	2-deoxy-2-[fluorine19]fluoro-D-glucose
FDG-MNPs	Silica and silane coated, PEGylated and FDG conjugated iron oxide magnetic nanoparticles
ICG	Indocyanine green
ICG@FDG-MNPs	ICG loaded FDG conjugated magnetic iron oxide nanoparticles
NPs	Nanoparticles
SPIONs	Superparamagnetic iron oxide nanoparticles
MNPs	Magnetic iron oxide nanoparticles

References

[1] S. K. Singh *et al.*, "Review of Photoresponsive Plasmonic Nanoparticles That Produce Reactive Chemical Species for Photodynamic Therapy of Cancer and Bacterial Infections", *ACS Appl Nano Mater*, vol. 6, no. 3, pp. 1508-1521, Feb. 2023, doi: 10.1021/acsanm.2c04551.

[2] G. Li, Z. Lai, and A. Shan, "Advances of Antimicrobial Peptide-Based Biomaterials for the Treatment of Bacterial Infections", *Advanced Science*, vol. 10, no. 11, p. 2206602, Apr. 2023, doi: https://doi.org/10.1002/advs.202206602.

[3] M. Abkar, S. Alamian, and N. Sattarahmady, "Gelatin Micro/Nanoparticles-Based Delivery of Urease and Omp31 in Mice Has a Protective Role Against Brucella melitensis 16 M Infection", *Bionanoscience*, vol. 13, pp. 1-9, Feb. 2023, doi: 10.1007/s12668-023-01073-6.

[4] U. Chilakamarthi and L. Giribabu, "Photodynamic Therapy: Past, Present and Future", *The Chemical Record*, vol. 17, no. 8, pp. 775-802, Aug. 2017, doi: https://doi.org/10.1002/tcr.201600121.

[5] Q. Zhang and L. Li, "Photodynamic combinational therapy in cancer treatment", *J BUON*, vol. 23, no. 3, pp. 561-567, 2018, [Online]. Available: http://europepmc.org/abstract/MED/30003719

[6] S. Perni, P. Prokopovich, J. Pratten, I. P. Parkin, and M. Wilson, "Nanoparticles: their potential use in antibacterial photodynamic therapy", *Photochemical & Photobiological Sciences*, vol. 10, no. 5, pp. 712-720, 2011, doi: 10.1039/C0PP00360C.

[7] S. Kwiatkowski *et al.*, "Photodynamic therapy-mechanisms, photosensitizers and combinations", *Biomedicine & Pharmacotherapy*, vol. 106, pp. 1098-1107, 2018, doi: https://doi.org/10.1016/j.biopha.2018.07.049.

[8] X. Wang *et al.*, "Analysis of the In Vivo and In Vitro Effects of Photodynamic Therapy on Breast Cancer by Using a Sensitizer, Sinoporphyrin Sodium", *Theranostics*, vol. 5, no. 7, pp. 772-786, 2015, doi: 10.7150/thno.10853.

[9] X. Dai, X. Li, Y. Liu, and F. Yan, "Recent advances in nanoparticles-based photothermal therapy synergizing with immune checkpoint blockade therapy", *Mater Des*, vol. 217, p. 110656, 2022, doi: https://doi.org/10.1016/j.matdes.2022.110656.

[10] D. Wang *et al.*, "Targeted Iron-Oxide Nanoparticle for Photodynamic Therapy and Imaging of Head and Neck Cancer", *ACS Nano*, vol. 8, no. 7, pp. 6620-6632, Jul. 2014, doi: 10.1021/nn501652j.

[11] M. Saeed, W. Ren, and A. Wu, "Therapeutic applications of iron oxide based nanoparticles in cancer: basic concepts and recent advances", *Biomater Sci*, vol. 6, no. 4, pp. 708-725, 2018, doi: 10.1039/C7BM00999B.

[12] C. Martinez-Boubeta *et al.*, "Learning from Nature to Improve the Heat Generation of Iron-Oxide Nanoparticles for Magnetic Hyperthermia Applications", *Sci Rep*, vol. 3, no. 1, p. 1652, 2013, doi: 10.1038/srep01652.

[13] B. Anegbe, I. H. Ifijen, M. Maliki, I. E. Uwidia, and A. I. Aigbodion, “Graphene oxide synthesis and applications in emerging contaminant removal: a comprehensive review”, *Environ Sci Eur*, vol. 36, no. 1, p. 15, 2024, doi: 10.1186/s12302-023-00814-4.

[14] K. Bin Liew *et al.*, “A review and revisit of nanoparticles for antimicrobial drug delivery”, *J Med Life*, vol. 15, pp. 328-335, Apr. 2022, doi: 10.25122/jml-2021-0097.

[15] J. Chomoucka, J. Drbohlavova, D. Huska, V. Adam, R. Kizek, and J. Hubalek, “Magnetic nanoparticles and targeted drug delivering”, *Pharmacol Res*, vol. 62, no. 2, pp. 144-149, 2010, doi: https://doi.org/10.1016/j.phrs.2010.01.014.

[16] E. Kianfar, “Magnetic Nanoparticles in Targeted Drug Delivery: a Review”, *J Supercond Nov Magn*, Jun. 2021, doi: 10.1007/s10948-021-05932-9.

[17] Q A Pankhurst, J Connolly, S K Jones, and J Dobson, “Applications of magnetic nanoparticles in biomedicine”, *J Phys D Appl Phys*, vol. 36, no. 13, p. R167, 2003, doi: 10.1088/0022-3727/36/13/201.

[18] Z. Yu *et al.*, “Reactive Oxygen Species-Related Nanoparticle Toxicity in the Biomedical Field”, *Nanoscale Res Lett*, vol. 15, no. 1, p. 115, 2020, doi: 10.1186/s11671-020-03344-7.

[19] P. Farinha, J. Coelho, C. Reis, and M. Gaspar, “A Comprehensive Updated Review on Magnetic Nanoparticles in Diagnostics”, *Nanomaterials*, vol. 11, p. 3432, Dec. 2021, doi: 10.3390/nano11123432.

[20] V. I. Shubayev, T. R. Pisanic, and S. Jin, “Magnetic nanoparticles for theragnostics”, *Adv Drug Deliv Rev*, vol. 61, no. 6, pp. 467-477, 2009, doi: https://doi.org/10.1016/j.addr.2009.03.007.

[21] E. Illés, E. Tombácz, M. Szekeres, I. Y. Tóth, Á. Szabó, and B. Iván, “Novel carboxylated PEG-coating on magnetite nanoparticles designed for biomedical applications”, *J Magn Magn Mater*, vol. 380, pp. 132-139, 2015, doi: https://doi.org/10.1016/j.jmmm.2014.10.146.

[22] O. J. Fakayode, N. Tsolekile, S. P. Songca, and O. S. Oluwafemi, “Applications of functionalized nanomaterials in photodynamic therapy”, *Biophys Rev*, vol. 10, no. 1, pp. 49-67, 2018, doi: 10.1007/s12551-017-0383-2.

[23] B. A. Thomas-Moore, C. A. del Valle, R. A. Field, and M. J. Marín, “Recent advances in nanoparticle-based targeting tactics for antibacterial photodynamic therapy”, *Photochemical & Photobiological Sciences*, vol. 21, no. 6, pp. 1111-1131, 2022, doi: 10.1007/s43630-022-00194-3.

[24] V. Yasakci, V. Tekin, O. Kozgus, V. Evren, and P. Unak, “Hyaluronic acid-modified [19F]FDG-conjugated magnetite nanoparticles: in vitro bioaffinities and HPLC analyses in organs”, *J Radioanal Nucl Chem*, vol. 318, Oct. 2018, doi: 10.1007/s10967-018-6282-6.

[25] M. Hu, G. Chen, L. Luo, and L. Shang, “A Systematic Review and Meta-Analysis on the Accuracy of Fluorodeoxyglucose Positron Emission Tomography/Computerized Tomography for Diagnosing Periprosthetic Joint Infections”, *Front Surg*, vol. 9, 2022, [Online]. Available: https://www.frontiersin.org/journals/surgery/articles/10.3389/fsurg.2022.698781

[26] Y. Yao *et al.*, “Nanoparticle-Based Drug Delivery in Cancer Therapy and Its Role in Overcoming Drug Resistance”, *Front Mol Biosci*, vol. 7, 2020, [Online]. Available: https://www.frontiersin.org/journals/molecular-biosciences/articles/10.3389/fmolb.2020.00193

[27] Y. Matsumoto *et al.*, “Evaluation of Multidrug Efflux Pump Inhibitors by a New Method Using Microfluidic Channels”, *PLoS One*, vol. 6, p. e18547, Apr. 2011, doi: 10.1371/journal.pone.0018547.

[28] C. Landon *et al.*, “Real-Time Fluorescence Microscopy on Living E. coli Sheds New Light on the Antibacterial Effects of the King Penguin β-Defensin AvBD103b”, *Int J Mol Sci*, vol. 23, no. 4, 2022, doi: 10.3390/ijms23042057.

[29] S. K. Gogoi, P. Gopinath, A. Paul, A. Ramesh, S. S. Ghosh, and A. Chattopadhyay, “Green Fluorescent Protein-Expressing Escherichia coli as a Model System for Investigating the Antimicrobial Activities of Silver Nanoparticles”, *Langmuir,* vol. 22, no. 22, pp. 9322-9328, Oct. 2006, doi: 10.1021/la060661v.

[30] E. Tutun, V. Tekin, V. Yasakcı, Ö. Aras, and P. Ünak, “Synthesis and morphological studies of Tc-99m-labeled lupulone-conjugated Fe3O4@TiO2 nanocomposite, and in vitro cytotoxicity activity on prostate cancer cell lines”, *Appl Organomet Chem*, vol. 35, no. 12, p. e6435, Dec. 2021, doi: https://doi.org/10.1002/aoc.6435.

[31] Y. Zhang, N. Kohler, and M. Zhang, “Surface modification of superparamagnetic magnetite nanoparticles and their intracellular uptake”, *Biomaterials*, vol. 23, no. 7, pp. 1553-1561, 2002, doi: https://doi.org/10.1016/S0142-9612(01)00267-8.

[32] M. Subramanian *et al.*, “A Pilot Study Into the Use of FDG-mNP as an Alternative Approach in Neuroblastoma Cell Hyperthermia”, *IEEE Trans Nanobioscience*, vol. 15, p. 1, Jul. 2016, doi: 10.1109/TNB.2016.2584543.

[33] K. L. Carraway and R. B. Triplett, “Reaction of carbodiimides with protein sulfhydryl groups”, *Biochimica et Biophysica Acta (BBA)-Protein Structure*, vol. 200, no. 3, pp. 564-566, 1970, doi: https://doi.org/10.1016/0005-2795(70)90112-1.

[34] C. Ozada, V. Tekin, F. B. Barlas, S. Timur, and P. Unak, “Protoporphyrin-IX and Manganese Oxide Nanoparticles Encapsulated in Niosomes as Theranostic”, *ChemistrySelect,* vol. 5, no. 6, pp. 1987-1993, Feb. 2020, doi: https://doi.org/10.1002/slct.201901620.

[35] V. Tekin *et al.*, “A novel anti-angiogenic radio/photo sensitizer for prostate cancer imaging and therapy: 89Zr-Pt@TiO2-SPHINX, synthesis and in vitro evaluation”, *Nucl Med Biol*, vol. 94-95, pp. 20-31, 2021, doi: https://doi.org/10.1016/j.nucmedbio.2020.12.005.

[36] B. Demir, F. B. Barlas, Z. P. Gumus, P. Unak, and S. Timur, “Theranostic Niosomes as a Promising Tool for Combined Therapy and Diagnosis: ‘All-in-One’ Approach”, *ACS Appl Nano Mater*, vol. 1, no. 6, pp. 2827-2835, Jun. 2018, doi: 10.1021/acsanm.8b00468.

[37] P. Kumar, A. V Ranawade, and N. G. Kumar, “Potential

Probiotic Escherichia coli 16 Harboring the Vitreoscilla Hemoglobin Gene Improves Gastrointestinal Tract Colonization and Ameliorates Carbon Tetrachloride Induced Hepatotoxicity in Rats", *Biomed Res Int*, vol. 2014, no. 1, p. 213574, Jan. 2014, doi: https://doi.org/10.1155/2014/213574.

[38] S. Moritake *et al.*, "Functionalized Nano-Magnetic Particles for an In Vivo Delivery System", *Journal Nanosci Nanotechnol*, vol. 7, pp. 937-944, apr. 2007, doi: 10.1166/jnn.2007.216.

[39] Y. Wang *et al.*, "Enhanced antimicrobial activity through the combination of antimicrobial photodynamic therapy and low-frequency ultrasonic irradiation", *Adv Drug Deliv Rev*, vol. 183, p. 114168, 2022, doi: https://doi.org/10.1016/j.addr.2022.114168.

[40] M. Ribeiro, I. B. Gomes, M. J. Saavedra, and M. Simões, "Photodynamic therapy and combinatory treatments for the control of biofilm-associated infections", *Lett Appl Microbiol*, vol. 75, no. 3, pp. 548-564, Sep. 2022, doi: https://doi.org/10.1111/lam.13762.

[41] R. Youf *et al.*, "Antimicrobial Photodynamic Therapy: Latest Developments with a Focus on Combinatory Strategies", *Pharmaceutics*, vol. 13, no. 12, 2021, doi: 10.3390/pharmaceutics13121995.

[42] D. Kunz, J. Wirth, A. Sculean, and S. Eick, "In-vitro-activity of additive application of hydrogen peroxide in antimicrobial photodynamic therapy using LED in the blue spectrum against bacteria and biofilm associated with periodontal disease", *Photodiagnosis Photodyn Ther,* vol. 26, pp. 306-312, 2019, doi: https://doi.org/10.1016/j.pdpdt.2019.04.015.

[43] V. Secchi, A. Monguzzi, and I. Villa, "Design Principles of Hybrid Nanomaterials for Radiotherapy Enhanced by Photodynamic Therapy", *Int J Mol Sci*, vol. 23, p. 8736, Aug. 2022, doi: 10.3390/ijms23158736.

[44] Y. K. Mohanta, K. Biswas, S. K. Jena, A. Hashem, E. F. Abd_Allah, and T. K. Mohanta, "Anti-biofilm and Antibacterial Activities of Silver Nanoparticles Synthesized by the Reducing Activity of Phytoconstituents Present in the Indian Medicinal Plants", *Front Microbiol*, vol. 11, 2020, [Online]. Available: https://www.frontiersin.org/journals/microbiology/articles/10.3389/fmicb.2020.01143

[45] O. Aras *et al.*, "An in-vivo pilot study into the effects of FDG-mNP in cancer in mice", *PLoS One*, vol. 13, p. e0202482, Aug. 2018, doi: 10.1371/journal.pone.0202482.

[46] F. Barlas *et al.*, "Multimodal Theranostic Assemblings: Double Encapsulation of Protoporphyrine-IX/Gd3+ in Niosomes", *RSC Adv*, vol. 6, Mar. 2016, doi: 10.1039/C5RA26737D.

[47] K. Bilici *et al.*, "Broad spectrum antibacterial photodynamic and photothermal therapy achieved with indocyanine green loaded SPIONs under near infrared irradiation", *Biomater Sci*, vol. 8, no. 16, pp. 4616-4625, 2020, doi: 10.1039/D0BM00821D.

[48] P. Magesan *et al.*, "Photodynamic and antibacterial studies of template-assisted Fe2O3-TiO2 nanocomposites", *Photodiagnosis Photodyn Ther*, vol. 40, p. 103064, 2022, doi: 10.1016/j.pdpdt.2022.103064.

[49] X. Cui *et al.*, "Charge adaptive phytochemical-based nanoparticles for eradication of methicillin-resistant staphylococcus aureus biofilms", *Asian J Pharm Sci*, vol. 19, no. 3, p. 100923, 2024, doi: https://doi.org/10.1016/j.ajps.2024.100923.

[50] S. F. Alanazi, "Evaluating the effect of X ray irradiation in the control of food bacterial pathogens", *J King Saud Univ Sci*, vol. 35, no. 1, p. 102367, 2023, doi: https://doi.org/10.1016/j.jksus.2022.102367.

[51] J. Cherif, A. Raddaoui, M. Trabelsi, and N. Souissi, "Diagnostic low-dose X-ray radiation induces fluoroquinolone resistance in pathogenic bacteria", *Int J Radiat Biol,* vol. 99, no. 12, pp. 1971-1977, Dec. 2023, doi: 10.1080/09553002.2023.2232016.

[52] V. Yemmireddy, A. Adhikari, and J. Moreira, "Effect of ultraviolet light treatment on microbiological safety and quality of fresh produce: An overview", *Front Nutr*, vol. 9, 2022, [Online]. Available: https://www.frontiersin.org/journals/nutrition/articles/10.3389/fnut.2022.871243

[53] O. Langer *et al.*, "Synthesis of fluorine-18-labeled ciprofloxacin for PET studies in humans", *Nucl Med Biol*, vol. 30, no. 3, pp. 285-291, 2003, doi: https://doi.org/10.1016/S0969-8051(02)00444-4.

[54] M. Silindir-Gunay and A. Y. Ozer, "99mTc-radiolabeled Levofloxacin and micelles as infection and inflammation imaging agents", *J Drug Deliv Sci Technol*, vol. 56, p. 101571, 2020, doi: https://doi.org/10.1016/j.jddst.2020.101571.

[55] A. Signore *et al.*, "Imaging Bacteria with Radiolabelled Probes: Is It Feasible?", *J Clin Med*, vol. 9, no. 8, 2020, doi: 10.3390/jcm9082372.

[56] J. Li *et al.*, "Effects of low-dose X-ray irradiation on activated macrophages and their possible signal pathways", *PLoS One*, vol. 12, p. e0185854, Oct. 2017, doi: 10.1371/journal.pone.0185854.

[57] A. Liebmann *et al.*, "Low-Dose X-Irradiation ofAdjuvant-Induced Arthritis in Rats", *Strahlentherapie und Onkologie*, vol. 180, no. 3, pp. 165-172, 2004, doi: 10.1007/s00066-004-1197-2.

[58] T. D. Luckey, "Physiological Benefits from Low Levels of Ionizing Radiation", *Health Phys*, vol. 43, no. 6, 1982, [Online]. Available: https://journals.lww.com/health-physics/fulltext/1982/12000/physiological_benefits_from_low_levels_of_ionizing.1.aspx.

[59] A. K. Lam *et al.*, "PEGylation of Polyethylenimine Lowers Acute Toxicity while Retaining Anti-Biofilm and β-Lactam Potentiation Properties against Antibiotic-Resistant Pathogens", *ACS Omega*, vol. 5, no. 40, pp. 26262-26270, Oct. 2020, doi: 10.1021/acsomega.0c04111.

[60] M. Bravo *et al.*, "Nanoparticle-mediated thermal Cancer therapies: Strategies to improve clinical translatability", *Journal of Controlled Release*, vol. 372, pp. 751-777, 2024, doi: https://doi.org/10.1016/j.jconrel.2024.06.055.

[61] J. M. Gillies, C. Prenant, G. N. Chimon, G. J. Smethurst, B. A. Dekker, and J. Zweit, "Microfluidic technology for PET radiochemistry", *Applied Radiation and Isotopes*, vol. 64, no. 3, pp. 333-336, 2006, doi: https://doi.org/10.1016/j.apradiso.2005.08.009.

[62] G. Unak *et al.*, “Gold nanoparticle probes: Design and in vitro applications in cancer cell culture”, *Colloids Surf B Biointerfaces*, vol. 90, pp. 217-226, 2012, doi: https://doi.org/10.1016/j.colsurfb.2011.10.027.

[63] L. M. V. Knappe Frederik Anton; Giovanella Luca; Luster Markus; Librizzi Damiano, “Diagnostic value of FDG-PET/CT in the diagnostic work-up of inflammation of unknown origin”, *Nuklearmedizin-NuclearMedicine*, vol. 62, no. 01, pp. 27-33, 2023, doi: 10.1055/a-1976-1765.

TURKISH ENERGY, NUCLEAR AND MINERAL RESEARCH AGENCY
TURKISH JOURNAL OF NUCLEAR SCIENCES
E-ISSN: 2791-7185
https://dergipark.org.tr/tr/pub/tjns

Thermal Hydraulics Safety Analysis at Steady State Operation of Burnup Core of TRIGA Mark II Research Reactor Utilizing PARET/ANL and COOLOD-N2

Md Altaf Hossen[1,*]

[1] **Reactor Physics and Engineering Division, Bangladesh Atomic Energy Commission, Ganakbari, Savar, Dhaka-1349, Bangladesh**

ARTICLE INFO

Article history:
Received November 25, 2024
Available online December 31, 2024

Research Article

Keywords:
• COOLOD-N2
• PARET/ANL
• Thermal hydraulics

ABSTRACT

Steady-state thermal hydraulics analysis of 700 MWD burned core of the TRIGA Mark II research reactor has been studied with the computational codes PARET/ANL and COOLOD-N2. This study aims to ensure the safety of burned TRIGA core by executing steady-state thermal-hydraulics calculations at full power. Fuel centerline temperature, fuel surface temperature, fuel clad temperature, DNB heat flux, and DNBR of the hottest rod, enthalpy, and coolant temperature have been calculated. Safety parameters from both codes align well, consistently maintaining margins significantly below the safety limits. Hence, PARET/ANL data from the simulation can be utilized for the transient study and core management of the reactor.

1. Introduction

Bangladesh Atomic Energy Commission has been operating TRIGA Mark II research reactor since its commission in 1986. The reactor is designed for multi-purpose uses, such as training, education, radioisotope production, and various R&D activities in neutron activation analysis, neutron scattering and neutron radiography [1]. The reactor, characterized by being light water-cooled and graphite-reflected, is specifically engineered for continuous operation at a constant power level of 3000 kW (thermal). An exceptional property of the TRIGA reactor lies in its well-demonstrated safety measures, primarily attributed to the substantial prompt negative temperature coefficient of reactivity inherent in its U-ZrH fuel-moderator composition. The reactor core comprises of 100 fuel elements, which include 5 fuel follower control rods and 2 instrumented fuel elements. The concentric hexagonal array design within the core shroud allows for efficient fuel distribution and optimal utilization of space in nuclear reactors. It is capable of functioning in both steady-state and pulsing modes, accommodating natural convection as well as forced convection cooling methods. Notably, the natural convection mode remains efficacious up to 500 KW, following which the transition to forced convection mode becomes imperative.

The prime goals of thermal hydraulics are to efficiently release the heat produced in the fuel without raising fuel temperatures too high or creating steam voids, and without getting too near to the hydrodynamic critical heat flux under steady-state operating circumstances. Since fission neutrons directly generate the reactor core's heat energy, there is a significant link between neutronic and thermal examination of the core. Hence, as the core undergoes burnup or any form of rearrangement, the power peaking factor of fuel rods and neutron flux distribution experience alterations, leading to changes in thermal hydraulics parameters like fuel centerline temperature and DNBR (Departure from Nucleate Boiling defined as the ratio of the critical heat flux to the heat flux achieved in the core). Therefore, it is imperative to analyse thermal hydraulics safety parameters in conjunction with burnup. The main purpose of conducting a thermal-hydraulic core analysis is to verify that the operating temperatures inside the core do not reach the design limit. By assuring that the greatest temperature detected in any fuel rod stays below the core design threshold, it may be fairly believed that the temperatures of the other fuel rods will similarly fall below acceptable ranges. Therefore, significant focus is put on monitoring whether the temperature of the hottest rod stays below the prescribed design threshold. Several algorithms have been used to calculate the thermal-hydraulic characteristics of the TRIGA Mark II research reactor in both steady-state and transient-state operations so far [2,3]. EUREKA has previously performed a simulation of the 700 MWD burned core of the TRIGA thermal hydraulics [4], using the Sudo-Kaminaga correlation for critical heat flux, the Dittus-Boelter correlation for single-phase flow, and the Chen correlation for two-phase flow [5]. General Atomic (GA), the vendor of the TRIGA Mark II reactor, recommended the utilization

*Corresponding author: altaf335@yahoo.com

of the Bernath correlation for DNBR calculation in the thermal hydraulics safety analysis due to its conservative nature [6]. Nevertheless, no thermal hydraulics burn-up analysis has been performed using the PARET/ANL code [7], which encompasses a wide array of correlations, particularly the Bernath correlation. In light of this, PARET/ANL has been utilized for this simulation employing Bernath correlation, with COOLOD-N2 [8] for comparative purposes. This study has simulated key safety parameters, specifically fuel centerline temperature, fuel surface temperature, fuel clad temperature, coolant temperature, enthalpy, DNB heat flux and DNBR to ensure the reactor operates within the safety margin. The ultimate purpose of this research is to utilize the PARET code for transient analysis for the present and modified core configurations.

2. Calculation Method

In thermal-hydraulic analyses, the term steady state in a reactor denotes a state where the reactor sustains a consistent power level that remains constant throughout its operation. The PARET/ANL and COOLOD-N2 code possess the capability to compute the heat transfer phenomena from the fuel element to the coolant when the reactor operates under steady-state conditions. The heat generation within the fuel core along the radial axis is assumed to be uniform, and a one-dimensional heat transfer models are employed in this codes. In this process, the distribution of temperatures along the axial direction of the fuel rods is determined based on the local bulk temperature of the coolant and axial peaking factors. Therefore, these two codes have been employed to calculate the steady state parameters of thermal hydraulics of the reactor. Figure 1 illustrates the configuration of the existing core of the reactor. Also, Table 1 represents significant thermal-hydraulic parameters of the reactor.

The power peaking factors of the 700 MWD burned core, used in this thermal hydraulics calculation, were determined using the Monte Carlo code MVP, incorporating the cross-section data library JENDL3.3 [9]. The calculation yielded the hottest rod factor of 1.668. Only peaking factor has been revised for simulating 700 MWD as no thermal properties have been reexamined here. Also physical parameters and operating condition for steady state operation for both BOC and 700MWD are same as the core arrangement is still the same. One other data that will be changed is reactivity and associated control rod insertion rate. However that will be applied in transient operation.

The axial peak-to-average power ratio at the hottest rod within the TRIGA core is presented in Figure 2. The thermal-hydraulic calculations were carried out with a water inlet temperature of 40.6˚C and an inlet pressure of 160.6 kPa, corresponding to the static pressure of water across the reactor channels. As per the final safety analysis report, the rate of mass flow for coolant circulation in the downward direction stands at 13248

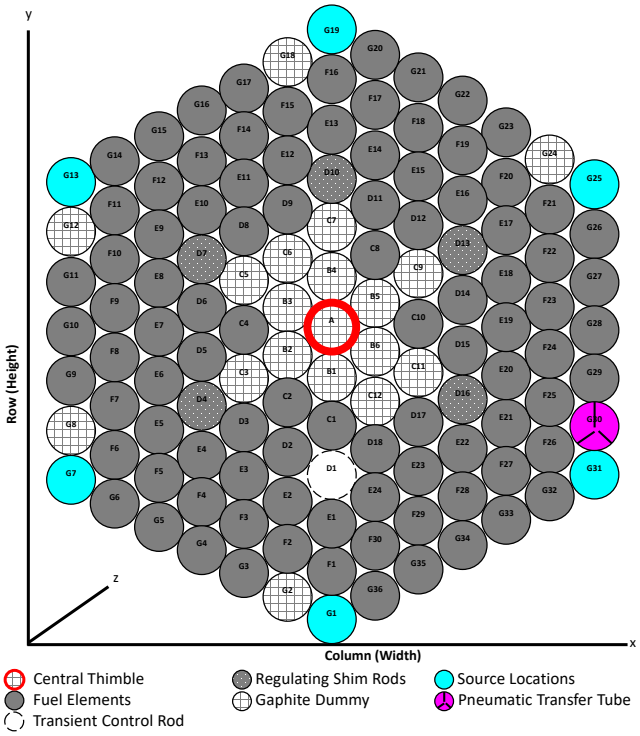

Figure 1. Present Core arrangement of TRIGA mark II research reactor.

liters per minute [10].

The PARET/ANL code was chosen due to general applicability, its simplicity of coding, and rapid execution. It is designed for use in predicting the course and consequences of non-destructive reactivity accidents in small reactor cores. It is a

Table 1. TRIGA fuel specifications.

Parameters	Design Vaue
Fuel Element (rod type)	20% w/o U-ZrH, 19.7% enriched
Total Number of fuels in the core	100
Cladding	Stainless Steel 304L
Reflector	Graphite
Inlet Temperature ˚C (Full Power)	40.6
Radius of Zr rod (cm)	0.3175
Fuel radius (cm)	1.82245
Clad outer radius (cm)	1.87706
Gap width (cm)	0.00381
Active fuel length (cm)	38.1
Flow area (cm^2)	5.3326
Hydraulic Diameter (cm)	1.80594
Pressure (Pa)	1.60654×10^5
Friction Loss Coefficient	0.07
Pressure Loss Coefficient	1.81(Inlet), 2.12 (Outlet)
Pitch (cm)	4.5716
Mass flow rate, kg/m^2s	3.2089×10^3
Coolant Velocity (cm/sec)	287.58

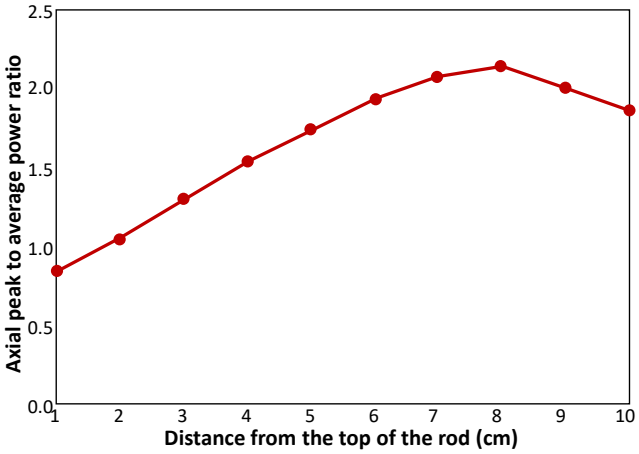

Figure 2. Axial peak to average power ratio.

coupled neutronic-hydro-dynamic heat transfer code employing point kinetics, one-dimensional hydrodynamics, and one-dimensional heat transfer. The kinetics equations of the point reactor ensure the dynamic behavior of power within the reactor through computational analysis. The time-dependent temperatures within the fuel element are computed using a one-dimensional heat conduction equation solved in axial sections. The resolution of these equations is accomplished by estimating the reactivity feedback from the initial moment until the specific point of interest. The feedback resulting from the expansion of fuel rods, the density effects of the moderator, and the fuel temperature effect collectively contribute to the overall reactivity feedback. The PARET/ANL model consists of a water-cooled core represented by a maximum of fifteen fuel elements and associated coolant channels. In our modelling the whole core was divided into two channels, keeping the hottest rod and associated coolant in one channel and other fuel and coolants in another channel. All channels were divided into 10 equal nodes. The Bernath correlation was chosen for the calculation of DNBR in this instance, as it yields the minimum value in accordance with the recommendations put forth by GA.

The COOLOD-N2 code is utilized for research reactors employing both plate-type and rod-type fuels. It can calculate fuel temperatures for both forced convection and natural convection cooling modes. The heat transfer coefficient and the DNB heat flux are determined using the Heat Transfer Package and Lund Correlation within this code. Power distribution at ten equal nodes along only the hottest rod was utilized in its modeling.

3. Results And Discussions

3.1. Axial Temperature Profiles

Steady-state thermal hydraulics parameters such as fuel centerline temperature, fuel surface temperature, fuel clad temperature along the axial length of 38.1 cm of the fuel, and coolant temperature have been studied in this simulation utilizing both PARET/ANL and COOLOD-N2. Data were taken at the center of the 10 equal axial nodes. All temperature profiles, such as fuel centerline temperature, fuel surface temperature, clad temperature, and coolant temperature, displayed an ascending trend from the top of the rod where it touches the peak just below the axial center, then gradually decreased towards the rod's end for both codes, as shown in Figure 3.

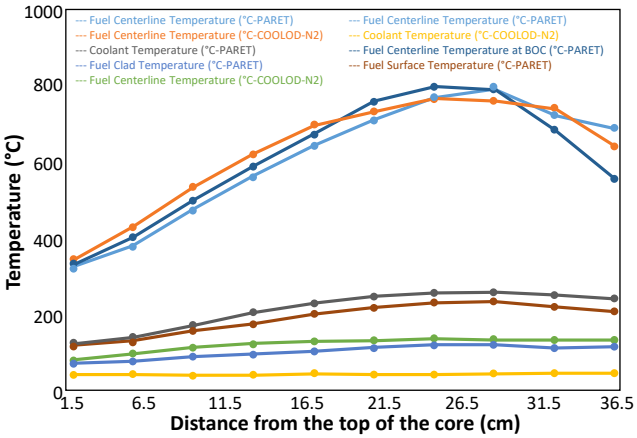

Figure 3. Temperature of the hottest channel at 750 MWD burned core

The analysis revealed that in the case of the PARET/ANL code, the fuel centerline temperature varied from 324.88°C at the topmost point to 678.48°C at the down most point, reaching its pinnacle at 770.03°C at position 28.57 cm from the top, while for COOLOD-N2, it ranges from 329.02°C to 636.68°C with a peak of 763.71°C at the same position. It was observed in another calculation that for the Beginning of Cycle (BOC) core, the PARET/ANL simulation spanned from 330.99°C to 552.26°C with a peak of 793.41°C at 24.76 cm from the peak. Hence, as the power peaking factor at burnup decreased, fuel centerline temperature profile also followed it.

The fuel surface temperature exhibited a similar pattern; it ascended from the upper region, reaching its maximum near the peak centerline temperature position, then gradually decreased towards the bottom. In the context of the PARET/ANL code, the temperature initiated at 114.50°C and culminated at 211.87°C, with a peak of 236.90°C. On the other hand, the fuel surface temperature in the COOLOD-N2 code ranged from 112.7°C to 236.15°C, with a peak of 254.69°C.

In another calculation, in the case of the PARET/ANL code, the clad temperature began at 73.63°C at the upper node, showing an upward trend until it reached the peak of 126.67°C at 24.76 cm, then decreased to 116.58°C at the lower node. Similarly, the COOLOD-N2 temperature profile mirrored the PARET/ANL results, starting at 83.09°C at the top, peaking at 133.52°C, and then declining to 127.05°C at the bottom. Hence, concerning both the maximum fuel surface temperature and the peak clad temperature, COOLOD-N2 exhibits

an overestimation when compared to PARET.

Subsequently, the coolant temperature commenced at 40.58°C at the top, exhibiting a nearly consistent increase until it reached 47.38°C at the end for PARET/ANL, while starting at 40.76°C at the top and rising to 46.59°C at the bottom for COOLOD-N2.

It is observed that among the four profiles, the fuel centerline temperature profile stood out the most, with PAREL/ANL showing an overestimation of the peak centerline temperature in comparison to COOLOD-N2. Only a limited amount of nucleate boiling is observed between the axial positions of 24.76 and 28.57 cm from the top, which is consistent with the Beginning of Cycle (BOC) outcomes [11]. However, peak temperatures from both codes are well below the fuel swelling temperature limit of 950°C as per SAR and are comparatively lower than the peak value for the BOC core, implying the burned core is safer than the BOC core.

It is also noted that all profile peaks were found just below the axial center. Ideally, flux distribution in fuels supposed to be in cosine shape over the axial length as neutrons in axial central gets moderated more than in the peripheral region. However, as coolant passes through the channel from the top, it takes heat from the fuel and get heated. As coolant comes down, its temperature increases. More importantly, it faces more heated fuel. As a consequence, the capacity of coolant to transfer heat from fuel reduces over axial length from the top. Therefore the right side of the cosine shape, due to lower part of the fuel, lifted slightly leaving the peak just down the axial center.

3.2. DNB Heat Flux and DNB Ratio

DNB heat flux and DNBR stand out as crucial parameters. To prevent the most adverse combination of mechanical and coolant conditions within the core, it is imperative to maximize the value of DNBR from unity as outlined in the Safety Analysis Report (SAR). DNB heat flux and DNBR calculation have been performed utilizing both codes [Figure 4 and Figure 5].

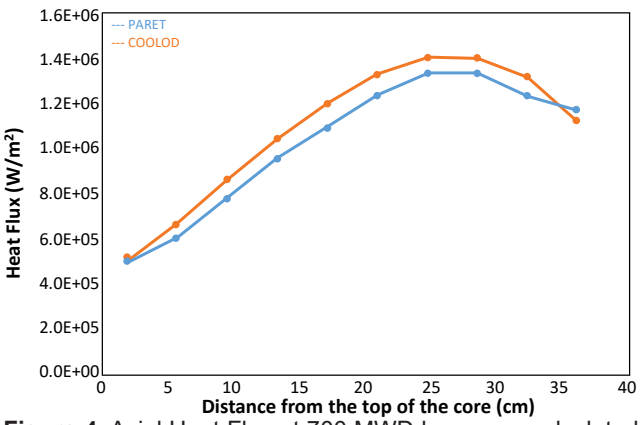

Figure 4. Axial Heat Flux at 700 MWD burn core calculated by COOLOD-N2 and PARET/ANL codes at 3 MW power.

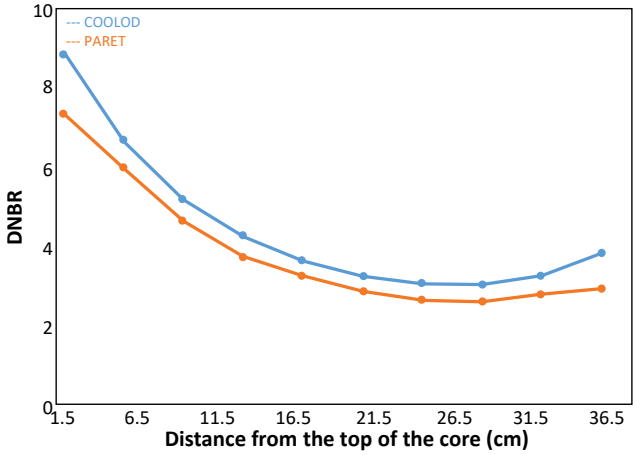

Figure 5. DNBR profile at 700 MWD burn core calculated by COOLOD-N2 and PARET/ANL codes at 3 MW power.

The DNB heat flux varies from 5.01×10^5 to 1.17×10^6 W/m^2 from the uppermost to the lowermost points, peaking at 1.35×10^6 W/m^2 at 28.57 cm for PARET. In comparison, it ranges from 5.05×10^5 W/m^2 to 1.11×10^6 W/m^2 with a maximum of 1.41×10^6 W/m^2 at the same position for COOLOD-N2. The DNBR spectrum for PARET/ANL was computed to be 7.39 at the topmost point, progressively decreasing until reaching its minimum value of 2.61 at 24.76 cm. It then rises to 2.96 at the lowest point. On the other hand, for COOLOD-N2, the DNBR ranges from 8.93 to 3.85, with a peak of 3.04.

As the DNB heat flux aligns with the enthalpy in the hottest rod, it escalates in the axial direction from top to bottom, culminating at the center for both codes. Similarly, the DNBR displays an inverse pattern as it represents the ratio of the DNB heat flux to the critical heat flux, with the minimum value corresponding to the maximum DNB heat flux. Consequently, PARET/ANL tends to overestimate the DNB heat flux compared to COOLOD-N2, while the opposite holds for the DNBR. It is also bigger than SAR accepted minimum value. Hence, our minimum DNBR values from both codes remarkably surpass that of EUREKA-2R and SAR, underscoring the core's safety at an operating power of 3MW.

3.3. Enthalpy

Also, the enthalpy within the fuel rod was determined solely using PARET/ANL, presented in Figure 6, as COOLOD-N2 does not offer this capability. Throughout the core's length, a consistent increasing trend is observed, commencing at 169.52 Kj/Kg and culminating at 197.94 Kj/Kg.

4. Conclusions

The thermal-hydraulic safety analysis of the 3 MW TRIGA Mark-II research reactor at Savar, Dhaka, Bangladesh has been evaluated using COOLOD-N2 and PARET/ANL. The computational outcomes of both cores were compared, revealing a high degree

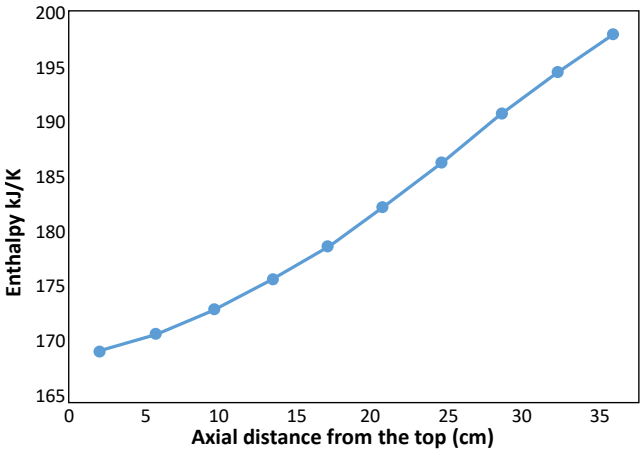

Figure 7. Enthalpy calculated by PARET/ANL.

of consistency between the two. Based on these findings, it can be inferred that the PARET/ANL and COOLOD-N2 codes exhibit a commendable capability in accurately predicting steady-state temperature profiles, enthalpy, DNB heat flux, and DNBR. Moreover, it is deduced that all safety parameters maintain margins well below the safety limits. Thus, the burned core of 3 MW TRIGA Mark-II research reactor is safer to operate compared to the BOC core. Therefore, the utilization of the PARET/ANL code is recommended for conducting transient analyses of the burned core, as well as for any modifications to the TRIGA core design.

References

[1] Hossain, S. M., Zulquarnain, M. A., Kamal, I. and Islam, M.N. Current Status and Perspectives of Nuclear Reactor Based Research in Bangladesh, IAEA, Vienna, (2011), 7-14. IAEA-TECDOC-1659

[2] Mizanur Rahman M. M., Akond M. A. R., Basher M K., and Huda M. Q., Steady State Thermal Hydraulic Analysis of TRIGA Research Reactor, World Journal of Nuclear Science and Technology, (2014), 81-87. DOI: 10.4236/wjnst.2014.42013

[3] Huda M. Q. and Rahman M., Thermo-Hydrodynamic Design and Safety Parameter Studies of the TRIGA MARK II Research Reactor, Annals of Nuclear Energy, 31, (2004) 1101-1118. https://doi.org/10.1016/j.anucene.2004.02.001

[4] Altaf M. H. and Badrun N. H., Thermal Hydraulic Analysis of 3 MW TRIGA Research Reactor of Bangladesh Considering Different Cycles of Burnup, Atom Indonesia, 40 (2014) 107-112. DOI:10.17146/aij.2014.328

[5] Sudo, Y., Ikawa, H. and Kaminaga, M, Development of Heat Transfer Package for Core Thermal Hydraulics Design and Analysis of Upgradded JRR-3. Proceedings of the International Meeting of Reduced Enrichment for Research and Test Reactors, Petten, (1985) 363-372.

[6] General Atomics, 10 MW TRIGA-LEU Fuel and Reactor Design Description. General Atomics, San Diego (1979).

[7] Obenchain, C.F., PARET—A Program for the Analysis of Reactor Transients. IDO-17282, Idaho Atomic Energy, 1969.

[8] Kaminaga, M., COOLOD-N2: A Computer Code, for the Analyses of Steady-State Thermal Hydraulics in Research Reactors, JAERI Report. Japan Atomic Energy Research Institute, Tokai-mura, Ibaraki, 1994.

[9] Mahmood M. S. et al., Individual Fuel Element Burnup of BAEC TRIGA Core, Technical Report, INST-RPED-RARD-01/009 (2012).

[10] FSAR, Final Safety Analysis Report for 3 MW TRIGA MARK-II Research Reactor at AERE, Savar, Dhaka, Bangladesh. BAEC, Dhaka (2006).

[11] Huda, M. Q., Bhuiyan, S. I., Chakroborty, T.K., Sarker, M.M. and Mondal, M.A.W. Thermal Hydraulic Analysis of the 3 MW TRIGA MARK-II Research", Reactor. Nuclear Technology, 135, "(2001), 51-66. https://doi.org/10.13182/NT01-A3205.

YAZAR KILAVUZU

GENEL BİLGİLER

• Makale başvurusu için Makale Metni Dosyası, Telif Hakkı Devir Dosyası ve Benzerlik Oran Dosyası olmak üzere üç ayrı formun doldurulması ve sisteme yüklenmesi gerekmektedir.
• Başvurularda iletişimde bulunulacak yazar ve diğer yazarların iletişim bilgileri bulunmalıdır.
• Makale metni içerisindeki makale kontrol listesi ve kapak sayfası eksiksiz olarak doldurulmalıdır.
• Makale metni dosyası içerisinde bulunan makale kontrol listesi ve kapak sayfası eksiksiz doldurulmalıdır.
• Derleme makalelerde başka yayınlara ait şekil ve tablolar kullanılacaksa, kaynak gösterilecek makalenin yayıncısından izin alınmalıdır. Yayıncıdan izin alındığı ve şekillerin uyarlanıp uyarlanmadığı veya doğrudan kullanılıp kullanılmadığı bilgisi şekil başlığında belirtilmelidir. İlgili izin yazısının journalofboron@tenmak.gov.tr adresine gönderilmesi gerekmektedir.
• Her makale, konusu ile ilgili en az iki hakeme gönderilerek şekil, içerik, özgün değer, uluslararası literatüre katkısı bakımından incelettirilir. Hakem görüşlerinde belirtilen eksikler tamamlandıktan sonra, son baskı formatına getirilir ve yazarlardan makalenin son halinin onayı alınır. Dergide basıldığı haliyle makale içinde bulunabilecek hataların sorumluluğu yazarlara aittir.

MAKALE METNİ DOSYASI

• Makale metninin yazımında yazım kurallarına uyulması gerekmektedir.
• Makale metninde kapsayıcı ve bilimsel bir dil kullanılmalıdır.
• Makale metni referanslar dahil araştırma makaleleri için 14.000 kelimeyi tarama makaleleri için ise 22.000 kelimeyi geçmemelidir.
• Makalenin metni, Times New Roman 12 punto ile Makale Metni Dosyası'nın sayfa düzeni değiştirilmeden yazılmalıdır.
• Makale metninin Microsoft Office Word 2010 ve üzeri bir kelime işlemci ile hazırlanması ve yazım hatalarının kontrol edilmesi ve düzeltilmesi gerekmektedir.
• Eğer makale Türkçe ise, Türkçe başlıklarla bire bir uyumlu olacak şekilde oluşturulmuş İngilizce başlıklar parantez içerisinde yazılmalıdır.
• Makale içerisinde kullanılan kısaltma ve sembollerin anlamları ilk kullanıldıklarında açıklanmalıdır.
• Makale metni içerisindeki alt başlıklar numaralandırılmalıdır. Numaralandırma işlemleri ana bölümler için 1.'den başlamalı ve tüm ana başlıklar (Özet, Teşekkür ve Kaynaklar ve Ekler bölümleri hariç) için devam etmelidir. İkincil başlıklar ana bölüm numaralandırmasına uygun olarak 1.1., 1.2., 1.3., ... şeklinde devam etmelidir. Üçüncü başlıklar ikinci başlıklara uygun olarak 1.1.1., 1.1.2., 1.1.3., ... şeklinde devam etmelidir.

TELİF HAKKI DEVİR DOSYASI

• İmzalı Telif Hakkı Devir Dosyası taranarak sisteme yüklenmelidir.
• İmzalı Telif Hakkı Devir Dosyası'nı göndermeyen yazarların başvuruları değerlendirmeye alınmaz.

BENZERLİK ORAN DOSYASI

• Makalenin referanslar bölümü hariç metni "iThenticate" veya "Turnitin" programları ile taranmalıdır.
• Benzerlik oranı raporunun PDF formatında sisteme yüklenmelidir.
• Benzerlik oranı %15'in üzerinde olmamalıdır.

GİZLİLİK POLİTİKASI

Journal of Boron gizliliğe saygı duymaktadır. Kişisel bilgiler, sadece derginin belirtilen amaçları doğrultusunda kullanılacak ve üçüncü kişilerle paylaşılmayacaktır.

YAZIM KURALLARI

MAKALE BAŞLIĞI
• Makale başlığı standart kısaltmalarla birlikte en çok 15 kelimeden oluşmalıdır.
• Eğer makale Türkçe ise, İngilizce başlıkla bire bir uyumlu olacak şekilde Türkçe makale başlığı da oluşturulmalıdır.

ÖZET
• Özet, 250 kelimeyi geçmemelidir.
• Standart olmayan kısaltmalar ilk kullanıldığında tam açıklamalarından sonra parantez içerisinde yazılmalıdır.
• Eğer makale Türkçe ise, İngilizce özetle bire bir uyumlu olacak şekilde Türkçe özet de oluşturulmalıdır.

ANAHTAR KELİMELER
• En fazla 5 anahtar kelime, alfabetik sıraya göre yazılmalıdır.
• Kısaltmalar anahtar kelime olarak kullanılmamalıdır.
• Eğer makale Türkçe ise, İngilizce anahtar kelimelerle bire bir uyumlu olacak şekilde Türkçe anahtar kelimelere de oluşturulmalıdır.

GİRİŞ
• İlgili literatürün özeti, çalışmanın amacı ve özgün değeri ve kurulmuş olan hipotezi içermelidir.
• Kaynaklar, toplu olarak ve aralıklı verilmemeli (örnek [1-5] veya [1, 2, 3, 5, 8]), her kaynağın çalışmaya katkısı irdelenmeli ve metin içerisinde belirtilmelidir.

MALZEMELER VE YÖNTEMLER
• Yürütülmüş olan çalışma deneysel bir çalışma ise deney prosedürü/metodu anlaşılır bir şekilde açıklanmalıdır.
• Teorik bir çalışma yürütülmüşse teorik metodu detaylı bir şekilde verilmelidir.
• Yapılan çalışmada kullanılan metot daha önce yayınlanmış bir metot ise diğer çalışmaya atıf yapılarak bu çalışmanın diğer çalışmadan farklı belirtilmelidir.

SONUÇLAR VE TARTIŞMA
• Elde edilen sonuçlar açık ve öz bir şekilde verilmelidir.
• Elde edilen tüm sonuçlar atıf yapılarak literatür ile karşılaştırılmalıdır.
• Tablolar numaralandırılmalıdır ve düzenlenebilir formatta olmalıdır. Eğer makale Türkçe ise, tablo üst yazılarının bire bir İngilizce çevirileri parantez içerisinde verilmelidir.
• Makale içerisindeki şekiller numaralandırılmalıdır ve en az 300 dpi çözünürlükte olmalıdır. Şekillerin üzerindeki yazılar okunabilir büyüklükte ve yazı tipinde olmalıdır. Kabul edilen şekil formatları TIFF, JPG ve JPEG'dir. Eğer makale Türkçe ise, şekil alt yazılarının bire bir İngilizce çevirileri parantez içerisinde verilmelidir.

SONUÇLAR
• Çalışmadan elde edilen ana sonuçlar ve çıkarımlar kısa ve öz bir şekilde verilmelidir.
• Çalışmaya ait gelecek perspektifleri bu bölümde verilir.

TEŞEKKÜRLER
• Çalışmanın gerçekleşmesi için sağlanan maddi kaynaklar ve kullanılan altyapı bu bölümde belirtilir.
Yazar Katkıları
• Her yazarın katkıları belirtilmelidir.
• Katkı rolleri şu şekildedir: kavramsallaştırma, veri analizi, veri iyileştirme, finansman sağlama, metodoloji, proje yönetimi, kaynak sağlama, yazılım analizi, denetim, doğrulama, görselleştirme, orijinal taslak yazma, inceleme yazma ve düzenleme.

KAYNAKLAR
• Basılmış kaynakların DOI ve ISBN numarası belirtilmelidir.
• İnternet sitesi adresleri (URL) kaynak olarak verilmemelidir. Ancak metin içerisinde istatistiksel bir verinin geçtiği yerde veriden sonra belirtilebilir.
• Kaynaklar listesi metin içerisinden kullanılma sırasına uygun olarak numaralandırılmalıdır.
• Kaynaklar, "APA Publication Manual, Seventh Edition" kurallarına uygun olarak hazırlanmalıdır.
• Kaynaklar İngilizce olarak hazırlanmalıdır. Türkçe kaynakların İngilizce karşılıkları köşeli parantez içerisinde belirtilmelidir.
• APA formatı ve örneklere aşağıdaki bağlantıdan ulaşılabilir.
https://apastyle.apa.org/style-grammar-guidelines/references/examples

EKLER
• Makaledeki ekler EK A (Appendix A), EK B (Appendix B) ve EK C (Appendix C) vb. olarak adlandırılmalıdır.
• Ekler içerisindeki denklemler A1, A2, A3 vb. olarak adlandırılmalıdır, tablo ve şekiller Tablo A1, Tablo A2, Şekil A1, Şekil A2 vb. olarak adlandırılmalıdır.

AUTHOR'S GUIDE

GENERAL INFORMATION

• For article application, 3 individual files which are Manuscript File, Copyright Transfer File and Similarity Ratio File, must be filled in and uploaded to the system.
• Applications should include the contact information of the author and other authors to be contacted.
• The article checklist and cover page in the Manuscript File should be filled in completely.
• Each article is sent to at least two referees related to its subject and examined in terms of format, content, novelty, contribution to literature.
• If figures and tables from other publications are to be used in review articles, permission must be obtained from the publisher of the article to be cited. The information that permission has been granted from the publisher and whether the figures have been adapted or used directly should be mentioned in the figure caption. The relevant permission letter should be sent to journalofboron@tenmak.gov.tr.
• After the deficiencies stated in the referee's comments are completed, it is brought to the final print format and the approval of the final version of the article is obtained from the authors. The responsibility of errors that may be found in the article as it is published in the journal belongs to the authors.

MANUSCRIPT

• Writing rules must be followed, during writing of the manuscript.
• Inclusive and scientific language must be used in the manuscript.
• Manuscript should not exceed 14,000 words for research articles and 22,000 words for review articles, including references.
• The manuscript should be written in Times New Roman 12 points without changing the page layout of the Manuscript File.
• The manuscript should be prepared with a word processor of Microsoft Office Word 2010 and above, and spelling errors should be checked and corrected.
• Abbreviations and symbols used in the manuscript must be explained when used fort he first time.
• Subheadings in the article should be numbered. Numbering should start at 1 for the main section and continue for all main headings (except the Summary, Acknowledgments and References and Appendices sections). Secondary titles continue as 1.1., 1.2., 1.3., ... in accordance with the main chapter numbering. The third headings continue as 1.1.1., 1.1.2., 1.1.3., ... in accordance with the second headings.

COPYRIGHT TRANSFER FILE

• Signed Copyright Transfer File should be scanned and uploaded to the system.
• Applications of the authors who do not send the signed Copyright Transfer File will not be evaluated.

SIMILARITY RATIO FILE

• The manuscript should be scanned with "iThenticate" or "Turnitin" programs, except for the references section.
• The similarity ratio report should be uploaded to the system in PDF format.
• The similarity ratio should not exceed 15%.

PRIVACY POLICY

Journal of Boron respects privacy. Any personal information will only be used in line with the stated purposes of the journal and will not be shared with third parties.

WRITING RULES

TITLE
• The title of the manuscript should consist of a maximum of 15 words with standard abbreviations.

ABSTRACT
• The abstract should not exceed 250 words.
• Non-standard abbreviations should be written in parentheses after their full explanation, when they are used for the first time.

KEYWORDS
• A maximum of 5 keywords should be written in alphabetical order.
• Abbreviations should not be used as keywords.

INTRODUCTION
• The summary of the relevant literature, aim and novelty of the study, and the established hypothesis should be included.
• References should not be given in bulk and in intervals (example [1-5] or [1, 2, 3, 5, 8]), the contribution of each source to the study should be examined and stated in the text.

MATERIALS AND METHODS
• If the study carried out is an experimental study, the test procedure/method should be clearly explained.
• If a theoretical study has been carried out, the theoretical method should be given in detail.
• If the method used in the study is a previously published method, the other study should be mentioned by citing.

RESULTS AND DISCUSSION
• Obtained results should be given in a clear and concise manner.
• All of the results should be compared with the literature by citing.
• Tables should be numbered and in editable format.
• Figures in the manuscript should be numbered and have at least 300 dpi resolution. The texts on the figures should be in legible size and font. Accepted figure formats are TIFF, JPG, and JPEG.

CONCLUSIONS
• Main conclusions and inferences obtained from the study should be given concisely.
• Future perspectives of the study are given in this section.

ACKNOWLEDGEMENTS
• The financial resources provided and the infrastructure used during the study are specified in this section.

AUTHOR CONTRIBUTIONS
• Contributions of each author must be stated.
• Contribution roles are as follows: conceptualization, data analysis, data curation, funding acquisition, methodology, project administration, sourcing, software analysis, supervision, validation, visualization, writing original draft, writing review and editing.

REFERENCES
• DOI and ISBN numbers of printed sources should be specified.
• Website addresses (URLs) should not be given as a source. However, it can be specified after the data where a statistical data is mentioned in the text.
• The list of references should be numbered according to the order in which they are used in the text.
• References should be prepared in accordance with the rules of “APA Publication Manual, Seventh Edition”.
• References should be prepared in English. English equivalents of sources should be indicated in square brackets.
• APA format and examples can be found at the link below.
https://apastyle.apa.org/style-grammar-guidelines/references/examples

APPENDICES
• Appendices in the manuscript must be named as Appendix A (Appendix A), Appendix B (Appendix B) and Appendix C (Appendix C) etc.
• Equations in the appendices must be named as A1, A2, A3, etc., and table and figures numberings must be named as Table A1, Table A2, Figure A1, Figure A2 etc.

TENMAK

TURKISH ENERGY, NUCLEAR AND MINERAL RESEARCH AGENCY

TURKISH JOURNAL OF NUCLEAR SCIENCES

E-ISSN: 2791-7185

https://dergipark.org.tr/tr/pub/tjns

İÇİNDEKİLER/CONTENTS

TENMAK Akademik Yayınlar Koordinatörlüğü

Ankara Üniversitesi Beşevler Kampüsü, Emniyet Mahallesi, Yenimahalle 06560, Ankara, Türkiye

Tel: (0312) 212 62 30

Fax: (0312) 295 87 61

E-posta: journal@tenmak.gov.tr

Web: https://dergipark.org.tr/tr/pub/tjns